Arabian Journal for Science and Engineering
https://doi.org/10.1007/s13369-024-09647-6

RESEARCH ARTICLE-MECHANICAL ENGINEERING

Effect of Heat Treatment on Corrosion Behavior of S275 Mild Steel Using Accelerated DC Voltage, LPR, and EIS

Liyamol Jacob[1] · Shahid Parapurath[1] · Nader Vahdati[2] · Ebru Gunister[3]

Received: 3 January 2024 / Accepted: 26 September 2024

Abstract
This study used an external DC voltage of 1.5 V to accelerate corrosion in heat-treated S275 mild steel samples at different time intervals. LPR and EIS were used to study the corrosion behavior of original and quenched steel samples. There was only a negligible difference in the corrosion rate (CR) for the original and the quenched samples up to 30 min of voltage application in a 3.5% NaCl electrolyte media. When the exposure time increased to 60 min, the original sample showed seven times higher CR than the quenched samples. The pits on the surface of the original samples acted as cathodes, enhancing the reaction rate on the surface and increasing its CR dramatically. This led to bimodal corrosion, where the first part is led by concentration and diffusion; while, the second part is led by localized corrosion. The smaller pits on the original surface samples served as cathodic reaction centers, exacerbating corrosion. The corrosion rate of the original samples ranged from 0.8 to 7.8 mmpy; whereas, the corrosion rate of the quenched samples remained consistently around 0.8 mmpy. This trend can be observed in long-term corrosion in different metals. The uniformly oriented martensitic microstructure and the quenched samples' small grain size prevented the enhanced ion penetration due to applied voltage. This study analyses the long-term stability of structural steel samples in marine environments by accelerating the corrosion rate by an applied external DC voltage.

Keywords Voltage accelerated corrosion · Microstructure · Heat treatment · EIS · Bimodal corrosion

1 Introduction

S275 mild steel, classified under the EN 10025 standard, represents a widely used construction material known for its balanced combination of mechanical properties and cost-effectiveness. Characterized by a minimum yield strength of 275 MPa, it finds extensive application in structural engineering, encompassing various load-bearing structures such as buildings, bridges, and machinery components [1]. Its composition primarily consists of iron and carbon, with small amounts of other elements such as manganese, sulfur, phosphorus, and silicon. The term "mild steel" refers to its relatively low carbon content, contributing to its malleability, weldability, and ductility [2]. This versatile material offers a suitable blend of strength, formability, and affordability, making it a cornerstone in engineering and construction disciplines where structural integrity and economic considerations intersect [3].

Corrosion, a vital aspect within engineering and material science, holds direct relevance to the characteristics of mild steel [4]. Corrosion can be defined as the gradual deterioration of materials due to chemical or electrochemical interactions with their environment. In the context of S275 mild steel, its structural applications often expose it to various corrosive agents, such as moisture, oxygen, and contaminants, which can compromise its integrity over time [5]. Understanding corrosion mechanisms, the factors influencing them, and their interplay with material properties is crucial for predicting the durability and longevity of

✉ Nader Vahdati
nader.vahdati@ku.ac.ae

1 Department of Mechanical Engineering, Khalifa University of Science and Technology, P.O. Box 127788, Abu Dhabi, United Arab Emirates

2 Department of Mechanical Engineering, Healthcare Engineering Innovation Center, Khalifa University of Science and Technology, P.O. Box 127788, Abu Dhabi, United Arab Emirates

3 Faculty of Engineering and Natural Sciences, Department of Mechanical Engineering, Istanbul Health and Technology University, 34445 Istanbul, Turkey

Published online: 11 October 2024

structures [6]. The composition, microstructure, and processing methods like quenching significantly impact the corrosion behavior of mild steel [7]. For instance, smaller grain sizes and uniform grain alignment can enhance corrosion resistance by reducing pathways for corrosive agents. Additionally, the presence of phases such as martensite can further influence the material's susceptibility to corrosion by altering its electrochemical properties. These effects however have not been elaborated in long-term corrosion, also the need for a short-term testing that would reflect the effect of long-term corrosion is critical. Managing corrosion through proper design, material selection, and protective coatings becomes imperative to ensure the extended service life of structures and components made from S275 mild steel. This continuity from material characteristics to the real-world corrosion challenges of corrosion underscores the practical significance of academic exploration in this field. For example, an accelerated corrosion process can be simulated by applying a controlled direct current to the steel sample in an electrochemical cell with a suitable electrolyte. This setup allows for continuous monitoring of the corrosion behavior through techniques such as electrochemical impedance spectroscopy (EIS). By analyzing the electrochemical data and examining the surface morphology over an extended period, researchers can predict long-term corrosion rates and mechanisms.

Corrosion research on metals in different environments provides direct data for developing mitigation strategies for aging structures. Natural corrosion can last decades [8]. Impressing direct current (DC) on steel samples in the laboratory can be used to partially corrode full-scale specimens within a short time and with limited resources [9]. The Electrolysis industry laid the foundation of voltage-induced corrosion acceleration. By attaching a specimen to the positive side of a DC power generator and a counter electrode to the negative side in an electrolyte solution, the specimen, i.e., the anode, undergoes oxidation reactions [10]. The applied voltage controls the reaction rate on the electrode surface. This technique can be used to accelerate the reaction on the surface, creating long-term corrosion within a short span of time [11].

Wang et al. [12] determined the effect of the applied spatial electric field (SEI) on the corrosion behavior of copper in a 3.5% NaCl solution. They applied a voltage of 8, 16.5, 25, and 32.5 V to generate different SEI and found that the voltage increased the corrosion rate dramatically. The corrosion weight loss with an exposure time of 180 min was 1.5 times that of the corrosion weight loss without applied voltage. This huge variation in corrosion rate is partly due to the complex nature of the exposure conditions and corrosion products. Parapurath et al. [13] studied the effect of heat treatment on the corrosion behavior of S275 steel under NaCl electrolyte. The authors found only a negligible difference in the corrosion rate due to heat treatment in the corrosion rate. However, this test did not account for the long-term corrosion behavior of steel. It is important to analyze the long-term effect of heat treatment in structural steel as they are employed in construction materials that ought to be long-lasting. It is also important to understand whether the corrosion mechanism also changes when a steel is used for longer period. The type of corrosion is quite critical to understand the damage of the steel employed. The same is true for long-term structural steel employed in concrete media. Kathler et al. [14] studied the enhanced corrosion in concrete media by accelerated chloride ion formation in reinforced concrete. Feng et al. [15] also conducted a similar study for rebars using accelerated corrosion. These studies have used high voltage to overcome the resistance from concrete media. By using a low voltage as in this research, we have focused on the effect of accelerated corrosion on the S275 mild steel's surface properties.

In this research, the application of DC was proposed to accelerate corrosion in S275 mild steel samples to understand the long-term effect of heat treatment. This is a simple method that can be used for studying the effect of corrosion mitigation mechanisms like coating and heat treatment on metal samples. The constant voltage facilitates the permeation of corrosive species throughout the steel surface, which promotes the corrosion process. In order to allow for comparison, a zero-voltage test was also conducted. Electrochemical Impedance Spectroscopy (EIS) and Linear Polarization Resistance (LPR) were utilized to measure the corrosion processes in the constant voltage and the zero-voltage tests. Optical microscopy was used to analyze the surface of the corroded materials and the extent of surface damage. Based on the results of the corrosion studies, conclusions were drawn on the corrosion mechanism and kinetics. As far as our knowledge, there are no studies conducted on the long-term effect of heat treatment on corrosion using an external voltage supply.

2 Materials and Methods

S275 mild steel was used for the corrosion studies. The temperature of the material was gradually raised to 600 °C at a speed of 10 °C per minute. Subsequently, it was maintained at this temperature for 30 min to allow for a period of stability. Following this, the material was then heated beyond the eutectoid temperature to reach 1000 °C, facilitating austenitization process. This heating was conducted at the same rate as before, with a dwell time of 45 min. The material was rapidly cooled to room temperature using a water bath, promoting microstructural changes without the involvement of diffusion. The Heat treatment cycle is as shown in Fig. 1. Following the heat treatment process and the subsequent

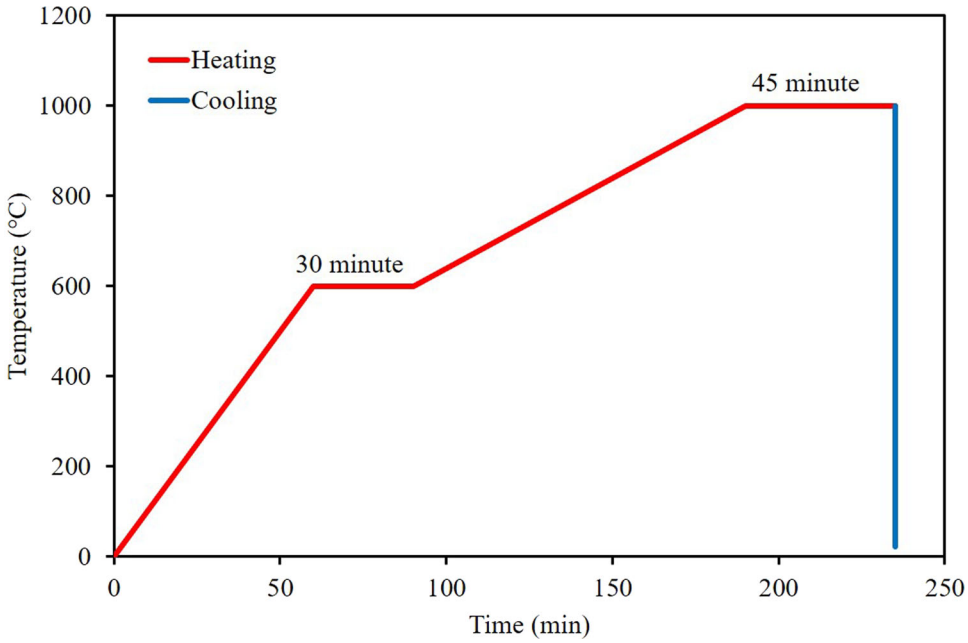

Fig. 1 Heat treatment cycle

shaping of the samples, their surfaces underwent grinding and polishing procedures. Four distinct phases of surface refinement were executed, each utilizing varying abrasive surfaces, to achieve specific levels of grinding and polishing. These stages encompassed coarse and fine grinding, as well as rough and fine polishing. The detailed process of sample preparation, heat treatment, and surface polishing is given in [13].

A schematic of the experimental set up is given in Fig. 2a. Using a two-electrode set up, a DC power supply of 1.5 V was applied to the samples, see Fig. 2b. The positive terminal was connected to the samples; while, the negative terminal was connected to a graphite electrode. The samples were immersed in a 3.5 wt% NaCl solution with an exposure time of 15, 30, 45, and 60 min. A control sample with no applied voltage was also maintained.

The samples were named O0, O15, O30, O45, O60, Q0, Q15, Q30, Q45, and Q60, where O and Q denote the original and the quenched samples, and the subsequent numbers denote exposure times. O0 and Q0 act as the control samples. Electrochemical data were obtained using LPR and EIS methods. LPR and EIS were conducted after applying the DC voltage for each interval and then switching it off. BioLogic VMP 300 potentiostat was used to study the electrochemical in a three-electrode cell. The working electrode was the sample, the reference electrode was Ag/AgCl, and the counter electrode was graphite. EIS measurements were conducted by application of sinusoidal voltage excitation of 5 mV in a frequency range of 100 kHz to 10 MHz for 10 points per decade, and LPR measurements were done with a scan rate of 0.1 mV/s in the voltage range of ± 20 mV. The data were then fitted using EC laboratory software. To ensure the credibility of the data, each test was triplicated with three samples of the same treatment, and the average value of the results was taken.

To observe the surface of the material after corrosion, optical microscopy was used. To observe the pits on the surface of the samples further, the layer of corrosion products was removed carefully, and the pit diameter and depth was calculated using an Alicona infinite focus 3D microscope. The rust formation was also observed using the same technique before removing the surface rust layer.

3 Results and Discussion

The corrosion rate of the materials was studied using the LPR technique. This method, combined with the application of a DC voltage for a specific time period, can provide a long-term corrosion rate within a very short period of time. Table 1 gives the LPR data derived from the test samples. The corrosion rate increases with the exposure time, as predicted. The original samples' corrosion rate is much higher than the quenched samples.

Figure S1 gives the LOG and LPR curves of the data. In the LOG curve a higher current density at a given potential suggests a higher corrosion rate. It provides detailed kinetics of the corrosion process, with Tafel slopes giving the corrosion current density and potential; while, the LPR curve indicates the resistance to polarization, with lower slopes suggesting higher corrosion rates. By analyzing the slopes of these curves, the polarization resistances (R_p) is calculated as

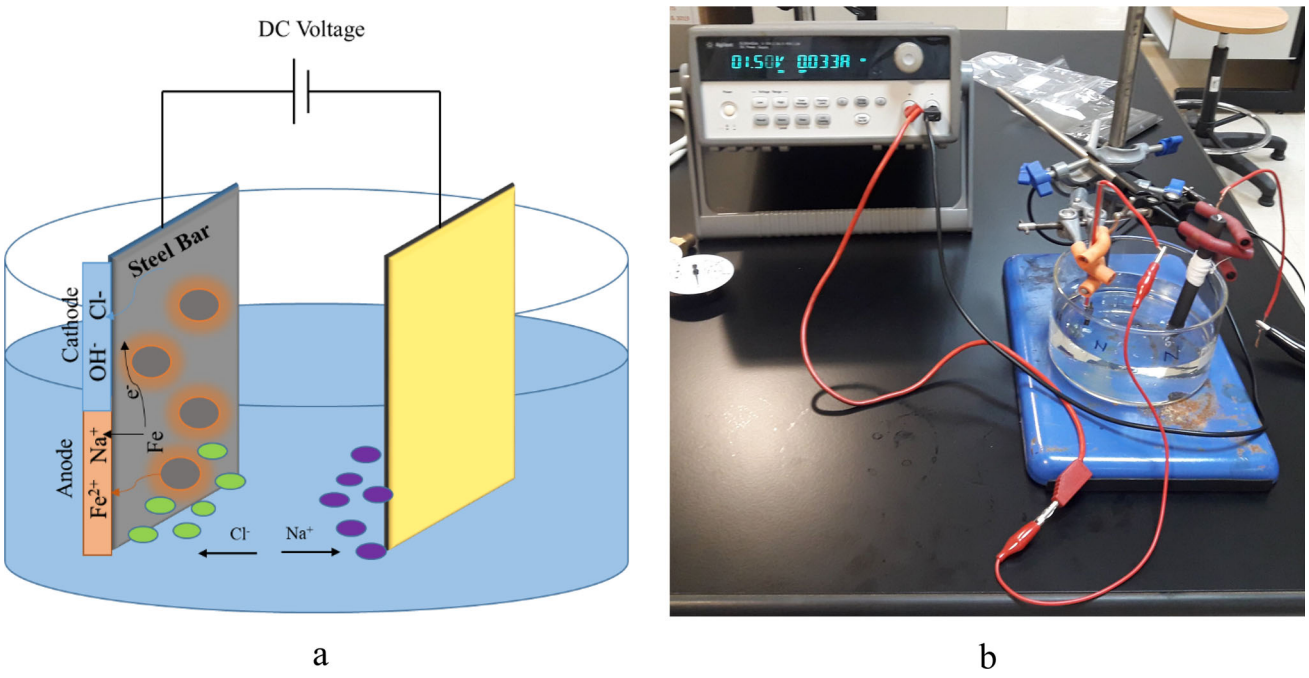

Fig. 2 **a** Schematics of the experimental setup **b** Actual experimental setup for voltage accelerated corrosion for S275 steel

Table 1 LPR data for the original (O) and the quenched (Q) samples in 1.5 V applied voltage at 0, 15, 30, 45, and 60 min

Sample	β_a mV	β_c mV	R_p Ωcm^2	E_{corr} mV vs Ag/AgCl	I_{corr} μAcm^{-2}	CR mmpy
O0	138.5	276.5	531	− 389.00	70.00	0.84 ± 0.034
O15	138.5	276.5	506	− 584.42	79.28	0.95 ± 0.041
O30	138.5	276.5	403	− 585.94	99.51	1.19 ± 0.023
O45	138.5	276.5	349	− 526.42	115.02	1.37 ± 0.031
O60	138.5	276.5	64	− 446.95	628.26	7.50 ± 0.021
Q0	120.6	236.8	527	− 386.00	54.00	0.65 ± 0.033
Q15	120.6	236.8	539	− 514.86	64.44	0.77 ± 0.024
Q30	120.6	236.8	486	− 568.25	71.49	0.85 ± 0.015
Q45	120.6	236.8	470	− 529.32	73.88	0.88 ± 0.031
Q60	120.6	236.8	437	− 527.28	79.46	0.95 ± 0.044

given in the table, which inversely correlates with the corrosion rate. The original samples have a CR of 0.95–7.50 mm/yr (mmpy), with an exposure time of 15–60 min. In the case of quenched samples, the CR varies from 0.77 to 0.95 mmpy. At 0 min and 15 min of voltage exposure, the difference in CR of both samples is negligible. This result agrees with [13] where the microstructure changes by heat treatment and its effect on CR was studied. As the exposure time increases, a significant change in corrosion rate can be seen. This may be because of microstructural changes due to quenching. The microstructural differences, such as grain boundary quantity and type, crystal orientation, and grain uniformity caused by quenching, greatly influence the corrosion resistance of S275 steel. In the martensitic quenched steel, the size of the carbides is much finer and well distributed. This phenomenon had been documented by researchers in a previous study [13]. The grain size also reduces with quenching. Katiar et al. found that this leads to low CR when compared with different microstructures in NaCl media [16]. In the beginning stages of corrosion, the corrosion protection layer formed was able to hold off corrosion for both the original and the quenched samples. However, with intensified corrosion due to the applied DC voltage, the ions penetrated the surface easily. However, the smaller grain size of the quenched samples can reduce ion penetration, causing long-term corrosion resistance [17]. This is particularly evident if the grain size is less than ~22 μm [18]. This, combined with the grain uniformity and crystal orientation [19] in the martensitic S275 quenched steel, caused an increase in corrosion resistance. It is also to be noted that generally in mild steel, an increase

in stress corrosion cracking as a result of quenching is not observed like in stainless steel [20].

EIS was used to determine the effect of applied voltage on the electrode surface. Figures 3a and b show the fitted Nyquist plots for O and Q samples under an applied voltage of 1.5 V. As explained earlier in Sect. 2, after applying the DC voltage for a specific time period, the DC voltage was turned off before collecting the EIS data. The impedance of all specimens was measured in 3.5 wt% NaCl at 0, 15, 30, 45, and 60 min of applied voltage exposure. Owing to the double layer interface between solution and the metal, all diagrams show a regular capacitive loop of a single semi-circle. Nyquist plots feature a typical single-capacitive semi-circle arc, representing an electrochemical process with only one time constant. The capacitive reactance's semi-circle radius decreased systematically as the time interval increased. This agrees with the increase in CR, according to LPR data. The steel electrode without a voltage (O0 and Q0) showed a large capacitive arc from Nyquist plots, signifying its largest impedance within the same test conditions. Figures 3c, d, e, and f presented measured Bode modulus and Bode phase angle plots for O and Q samples, respectively. The maximal phase angle and impedance value decreased with the increase in exposure time, similar to that of Nyquist curves. Furthermore, the Bode diagram showed two time constants in agreement with the equivalent circuit, showing two capacitive semi-circles with two close time constants overlapped in the Nyquist plot. Additionally, in the Bode diagram, the majority of the phase angles surpass $-45°$. This shows a uniform and continuous distribution of current density on the surface of the electrode in sodium chloride solution with the applied voltage [21].

The fitting of EIS data was done using a simple equivalent electric circuit model, as shown in Fig. 3a insert. The equivalent circuit diagram matches well with the experimental results. The electrochemical data after fitting are shown in Table 2, where n showed surface irregularity ($0 \leq n \leq 1$) if $n = 1$, it is a pure capacitor. If n is between 0.5 and 1, time constant distribution in frequency space is given by constant phase angle. Q_{dl} represented the electric double-layer capacitance, R_{ct} indicated charge transfer resistance, R_f and C_f were linked to the corrosion productfilm, and R_s signified solution resistance. By associating the results of R_f in Table 2, it can be seen that the surge in exposure time caused a decrease in R_f, until 45 min, where there is a sudden increase. The R_f value dropped again at 60 min. The disintegration of the corrosion protection film is the cause of the decrease in R_f at 15 and 30 min. As the oxide layer of iron oxides coats the surface, producing a rust layer [22], the irregularly formed pits join to form full coverage on the surface at 45 min, causing an increase in R_f. However, this product formation will not be sustainable due to the attack of Cl^- ions on the steel surface, disintegrating the rusted surface formed, showing the drop of R_f at 60 min. As the iron oxides formed on the surface are connected to the underlying metal, the pits could act like a cathodic area, reducing O_2 on the surface [23]. It causes a decoupling of anodic and cathodic reactions, as oxidation occurs on the metal in proximity to with the electrolyte under the pits, and reduction occurs on the cathodic area generated by the iron oxides [22]. This means the inhibitory influence of the oxide layer formation prevails the formation of iron dissolution with the increase in the size and quantity of pits. This formation reaches a maximum at 45 min, as the primarily formed pits that grow as distinct units become covered by an iron oxide cap. The same trend can be observed in both O and Q samples. However, the value of R_f was lower for quenched samples, relating to its low CR. O0 and Q0 samples showed the highest R_f as the corrosion protective film formed was the thickest. R_{ct} of steel showed a low value because of voltage addition. Due to the increase in exposure time, R_{ct} showed a decreasing trend and reached a minimum value at an exposure time of 60 min for all samples. The quenched samples had higher R_{ct}, indicating lower corrosion rates. The difference in the R_{ct} values of the quenched samples becomes more pronounced after 45 min of exposure time. The R_{ct} values halved after 45 min of exposure. An increase inimmersion time favors the development of a layer of oxide and/or chloride product on the surface to guard steel from corrosion attack further [24]. This, combined with smaller grain size and uniform grain orientation, decreased charge transfer resistance with increased exposure time. The results were ascribed to the effect of the applied voltage on the increased ion migration on the S275 surface in the sodium chloride solution, that which was steady with LPR results.

Figure 4 shows the surface coverage and pit formation as the reaction proceeds. Corrosion products fully cover both the original and the quenched samples at 60 min. However, the pits in the original samples are much larger and deeper.

In the case of the original samples, as time progresses, the pits combine to form deep grooves on the surface (Figs. 5a, b). Figure 5c shows the time dependence of corrosion rate with applied voltage. For the original sample, the trend is similar to bimodal corrosion observed in long-term corrosion of different metals in marine environments [25, 26]. Here, the corrosion proceeds in two phases. The first phase, 0–45 min, is based on diffusion and concentration gradient. After 45 min, localized corrosion seems to grow, affecting the overall corrosion rate. This is a result of rust build-up, which changes the aerobic conditions of the reactions to anaerobic reaction conditions where hydrogen evolution cathodic reaction is dominant. The anaerobic reactions lead to long-term corrosion, as the rust is maintained to preserve the anaerobic conditions at the metal corrosion–corrosion product interface [27]. This happens simultaneously as the pits become cathodic centers and the surrounding steel as an anode, promoting localized corrosion. The microscopic

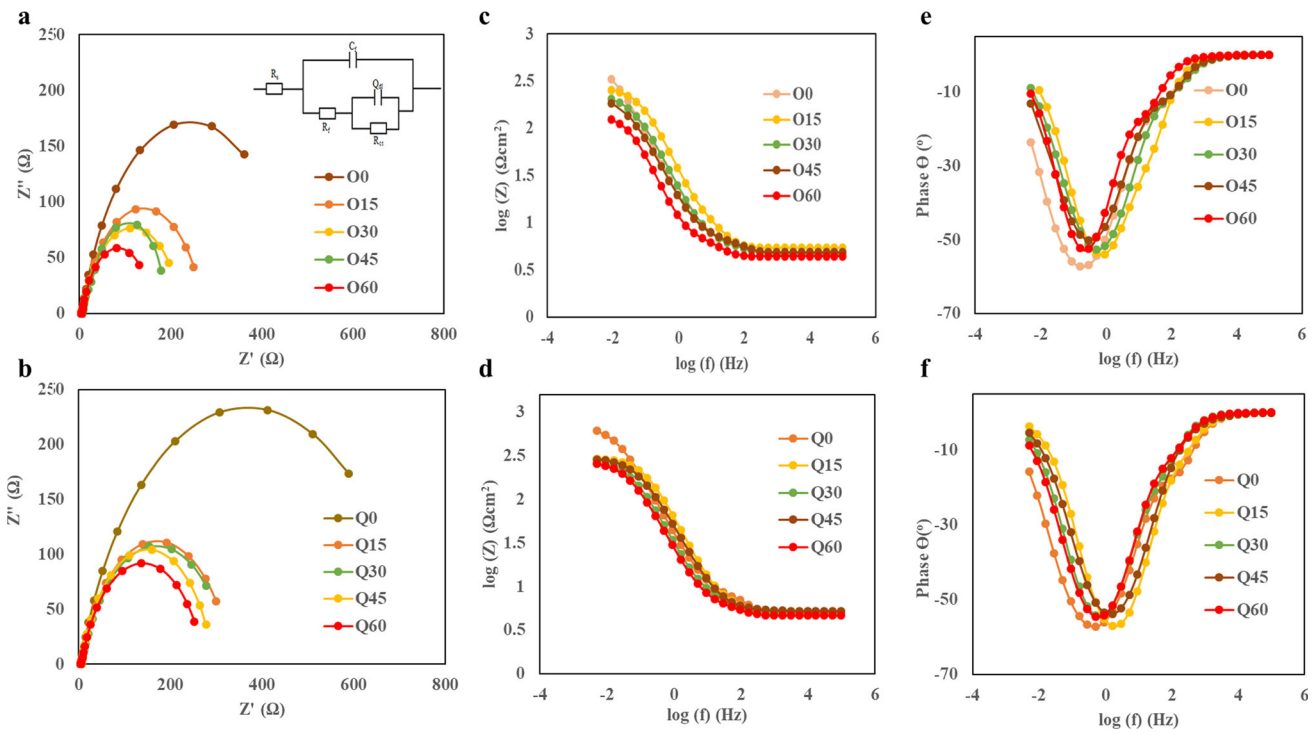

Fig. 3 **a** and **b**: Nyquist diagram for the original (O) and the quenched (Q) samples in 1.5 V applied voltage at 0, 15, 30, 45, and 60 min, **c** and **d**: Bode diagram for O and Q samples, **e** and **f**: Bode phase angle fit for O and Q samples. All curves are fitted

Table 2 Fitted electrochemical parameters for impedance spectra

Sample	R_s Ωcm^2	C_f Fcm^{-2}	R_f Ωcm^2	Q_{dl} snΩ^{-1} cm^{-2}	n	R_{ct} Ωcm^2
O0	5.27	4.93×10^{-3}	16.68	0.014	0.79	452.2
O15	5.39	1.30×10^{-3}	7.04	0.017	0.74	262.3
O30	4.74	1.97×10^{-3}	4.00	0.010	0.74	219.2
O45	5.09	4.23×10^{-3}	14.8	0.016	1.00	156.8
O60	4.43	2.47×10^{-3}	3.49	0.016	0.75	92.1
Q0	6.52	2.19×10^{-3}	9.64	0.005	0.64	745.4
Q15	5.10	9.56×10^{-3}	5.85	0.003	0.67	332.7
Q30	5.17	4.33×10^{-3}	5.91	0.005	0.72	311.2
Q45	5.28	2.06×10^{-3}	10.17	0.007	0.74	303.9
Q60	4.76	1.47×10^{-3}	3.00	0.008	0.74	265.8

images in Fig. 5a show deeper and thicker grooves on the original sample's surface, indicating its high corrosion losses. This is similar to the observation made by Melchers et al. [28, 29] in pit formation and corrosion losses in mild steel exposed to long-term marine corrosion. After the simulated DC application, the black corrosion product, due to the generation of magnetite (Fe_3O_4) and the red dust (Fe_2O_3), was seen on the anode [30].

The formation of corrosion products was further confirmed with Raman analysis (Figs. 6 a, b). At 15 min, there is no significant corrosion product formation for both the original and the quenched samples. An increase in exposure time results in more corrosion product formation, and the peaks become significant for both the original and the quenched samples. The corrosion products primarily consist of various oxides and oxyhydroxides. Depending on the corrosion medium, Fig. 6 indicate the presence of hematite (α-Fe_2O_3) [31], wustite (FeO), magnetite (Fe_3O_4), goethite (α-FeOOH), and lepidocrocite (γ-FeOOH) [32–34]. Specifically, the Raman spectra exhibit distinct peaks at 217 cm^{-1}, 285 cm^{-1}, and 1299 cm^{-1}, which correspond to hematite. Goethite and lepidocrocite are identified by peaks at 396 cm^{-1} and 489 cm^{-1}, respectively, with medium and

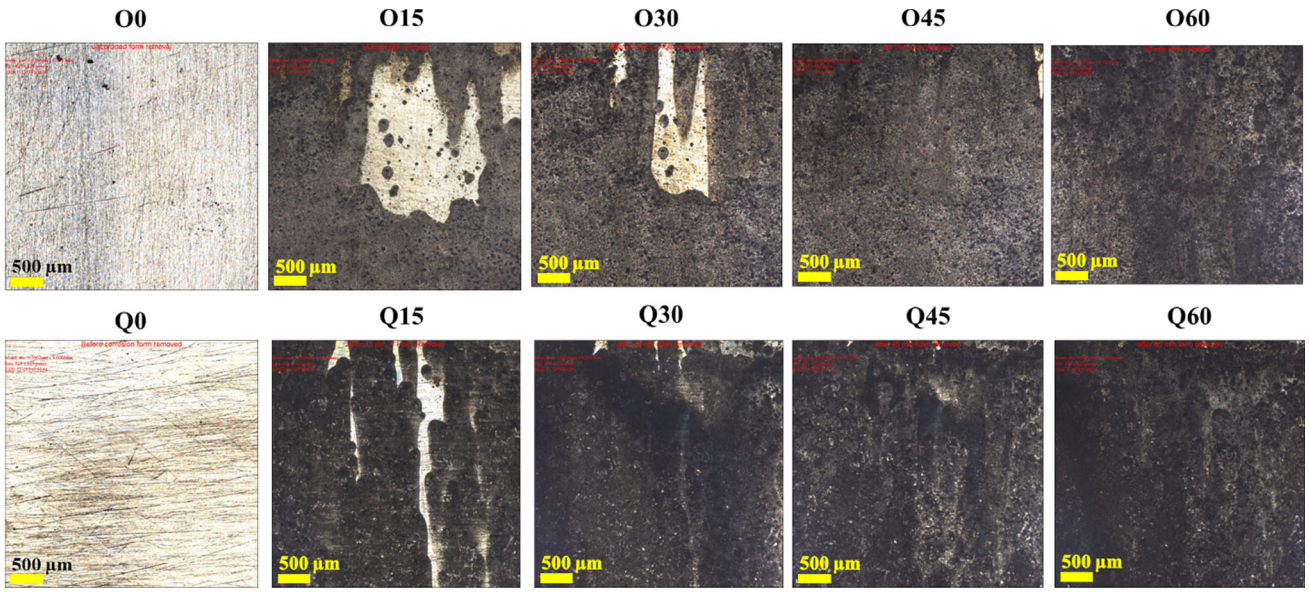

Fig. 4 Optical Microscopy images of the original (O) and the quenched (Q) samples at 0,15,30,45, and 60 min of 1.5 V applied voltage. All images are in 500 µm scale

low intensity. Additionally, minor shoulder peaks representing wustite and magnetite are observed at 599 cm^{-1} and 655 cm^{-1}. Fe_2O_3 can be formed by additional oxidation of $Fe(OH)_2$, precipitating an oxide layer on the S275 surface [33]. The formation of specific iron oxides and hydroxides during the corrosion of mild steel has significant implications for the material's integrity and longevity. Hematite (α-Fe_2O_3) is a stable and protective layer that can slow down further corrosion, but its formation indicates advanced rusting. Wustite (FeO), often an intermediate product, is unstable and can quickly convert to more stable oxides, suggesting active ongoing corrosion. Magnetite (Fe_3O_4) is a mixed valence oxide that can form under reducing conditions and is generally more protective than other oxides, though it still allows some corrosion. Goethite (α-FeOOH) and lepidocrocite (γ-FeOOH) are both common rust components; goethite provides some passivation; while, lepidocrocite is less protective and indicates a higher rate of corrosion [35, 36]. Identifying these products helps assess the corrosion stage and the effectiveness of protective measures.

The microscopy images can visualize the pitting phenomenon as given in Figs. 7a–d and e–h for the original and the quenched samples, respectively. The accelerated corrosion of steel samples with NaCl solution can be compared to a simple chlor-alkali manufacturing system for chlorine production [37]. This might cause the generation of NaOH in the electrolyte, imparting alkalinity to the sample. The chlorine gas generated also can cause a decrease in corrosion. However, this did not have any apparent effect on the corrosion rate as the oxidation reactions were aggressive, and with increased exposure time, CR continued to grow. Figure 7 shows that all samples show pitting corrosion with varying coverage of corrosion products depending on exposure time. The number of pits and size of pits increased with increase in time. This is more significant in the case of the original samples. The growth in the number of pits is much slower in the case of the quenched samples. These findings are in line with LPR results.

Figures 8a and b show the changes in pit diameter and pit depth of the original and the quenched samples. The original and the quenched samples show a quick increase in pit diameter after 45 min of exposure time. The pit diameter of the original sample is 20 µm after 60 min of exposure, whereas for the quenched samples, it is 15 µm. The pit depth shows higher variation depending on the exposure time. For the original samples, pit depth increased from 25 to 45 µm whereas for the quenched samples, pit depth increased from 12 to 22 µm. In the quenched mild steel, the heat treatment process involves rapid cooling from a high temperature to room temperature [13]. This rapid cooling prevents the formation of coarse and uneven microstructures, resulting in a finer and more uniform grain structure. This refined microstructure enhances the material's hardness, strength, and resistance to deformation and wear. As a result, when subjected to corrosive environments or abrasive forces that could create pits, the quenched mild steel is better equipped to resist these effects. The hardened microstructure provides a barrier against the penetration of corrosive agents or abrasive particles, leading to smaller pit sizes and shallower depths. On the other hand, non-heat-treated samples lack the benefits of the controlled microstructural changes that occur during heat treatment. These samples retain a comparatively coarser

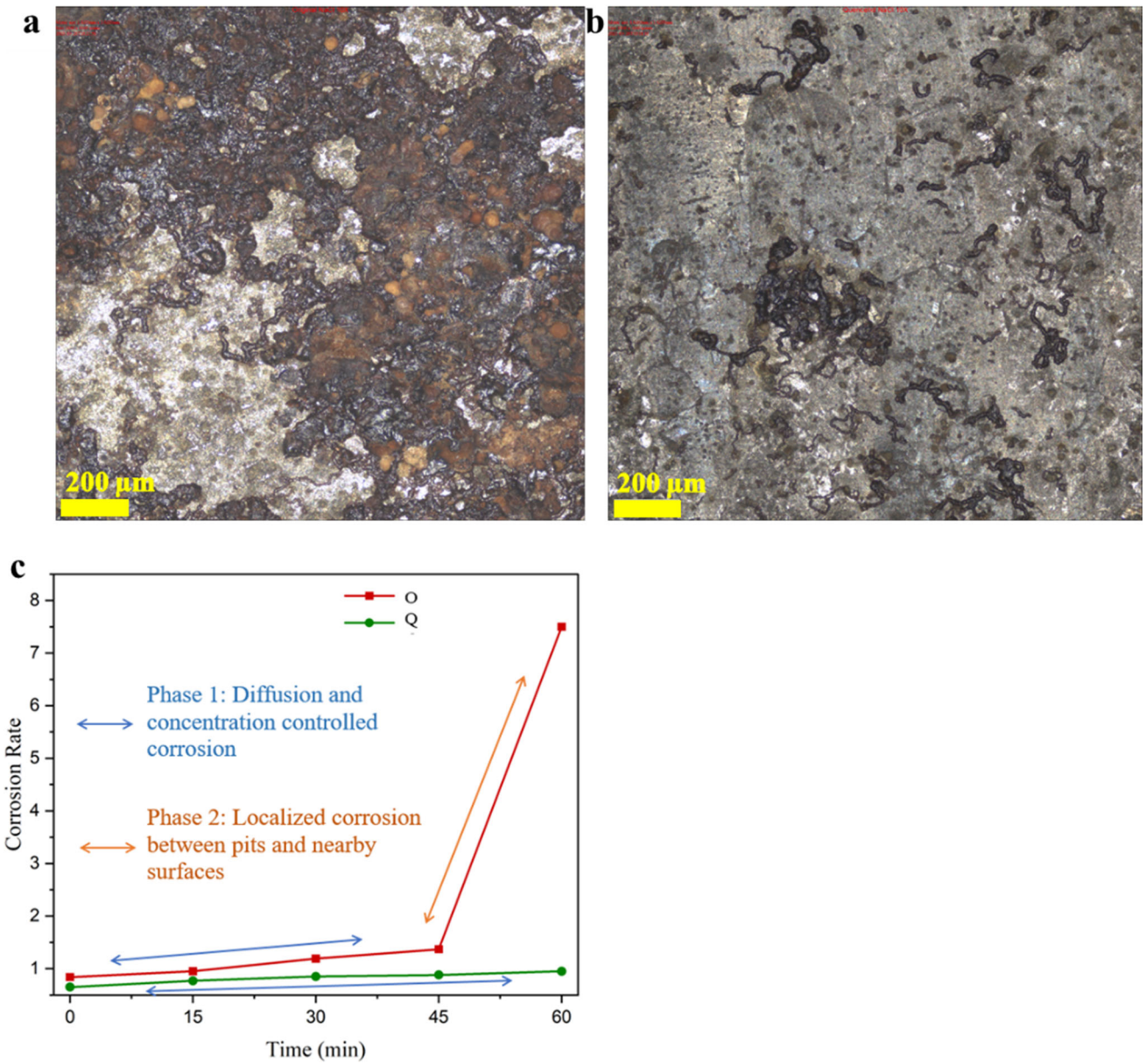

Fig. 5 **a** and **b**: Microscopic images of O and Q sample surface after 60 min of exposure in 200 µm scale, **c**: Corrosion rate vs. Time graph

and less uniform microstructure, which can be more susceptible to corrosion and abrasion. This susceptibility leads to easier penetration of corrosive agents and abrasive particles into the material's surface, resulting in larger pit sizes and greater depths over time. In both the quenched and the original samples, at 45 min, full coverage of the corrosion product can be seen. Withtime, the depth of the pits increases, indicating aggravated damage to the steel surface. Compared to the original samples, the quenched samples had shallower and smaller pit sizes. This corroborates the high corrosion rate of the original samples.

To summarize, applying an external voltage significantly impacts the corrosion behavior of S275 steel through electrochemical processes. When an external voltage is applied, it influences the kinetics of cathodic and anodic reactions occurring at the material's surface [15]. In a natural environment, where the steel is exposed to elements such as moisture, oxygen, and contaminants, the applied voltage can accelerate or impede the corrosion process. For instance, under anodic polarization (positive potential), the voltage can increase dissolution rates, leading to accelerated corrosion [38]. Conversely, cathodic polarization (negative potential) can hinder corrosion by reducing the driving force for anodic reactions. Furthermore, the voltage-induced changes in pH

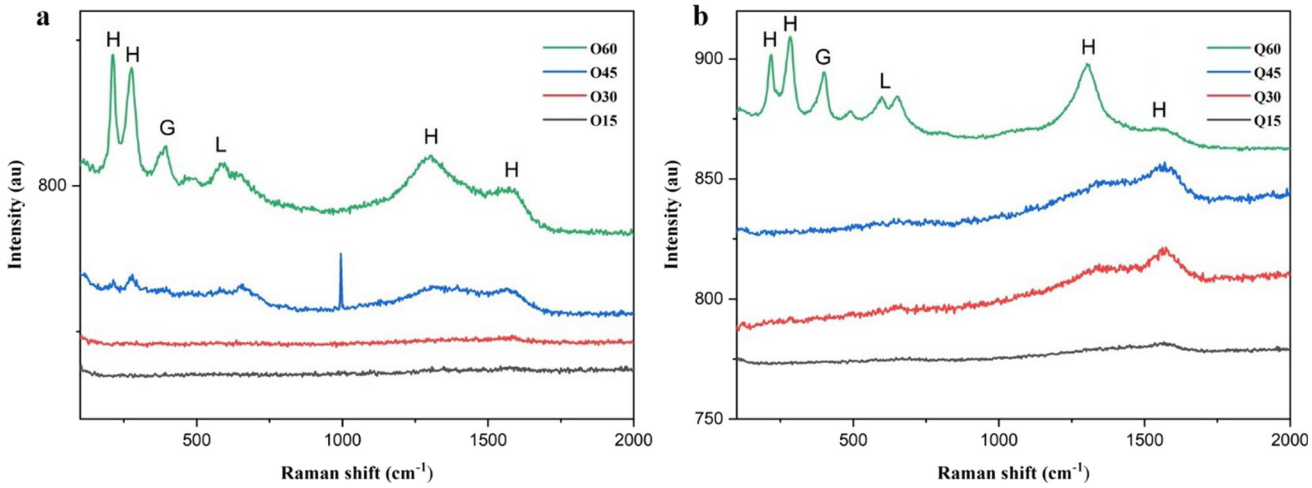

Fig. 6 Raman spectra of the **a** original and **b** quenched samples with respect to time

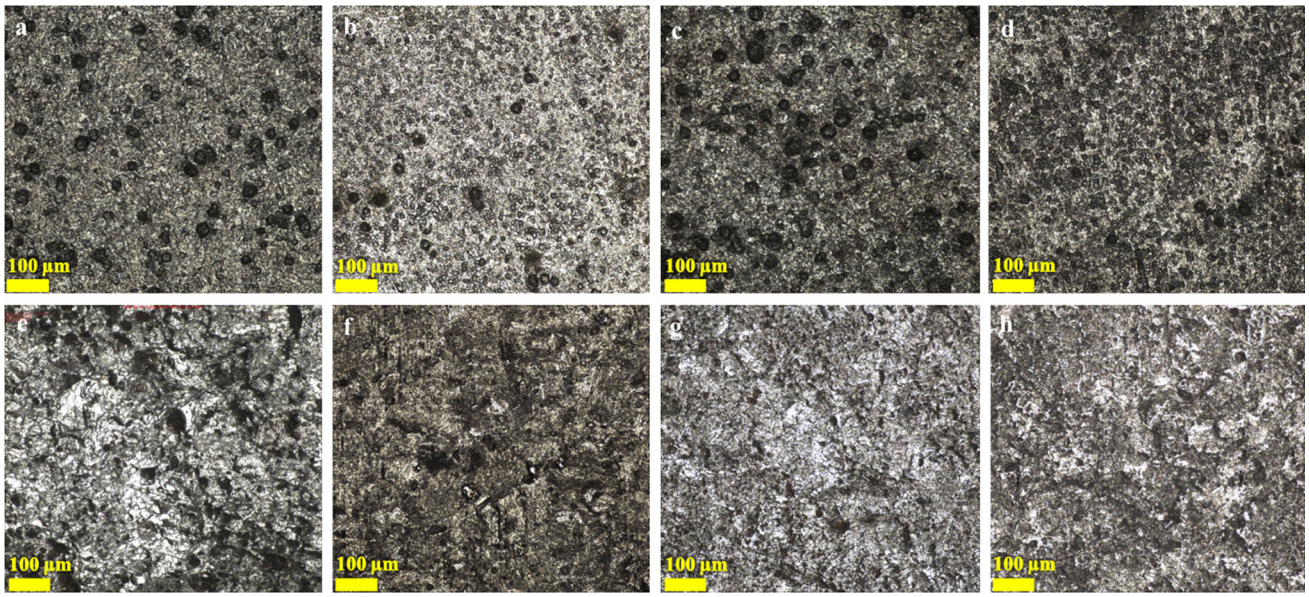

Fig. 7 **a**–**d** and **e**–**h** Microscopic images of pit formation on the original and quenched sample surface with respect to time. All images are in 100 µm scale

near the surface and alteration of passive film properties can impact the steel's susceptibility to localized corrosion. These electrochemical mechanisms, occurring in tandem with environmental factors, intricate material composition, and microstructure, collectively dictate the corrosion behavior of S275 steel in natural settings [39]. A comprehensive understanding of these interactions is essential for assessing the long-term durability of structures and materials in practical applications. Besides this, 1.5 V can occur due to stray electrical currents in the vicinity, faulty electrical grounding, or other sources of electrical potential around structural steel or in its environment. For instance, in marine environments, where chloride ions are abundant, the combination of 3.5% NaCl and 1.5 V can lead to localized pitting corrosion, general corrosion, or other forms of accelerated degradation [40]. This can compromise the integrity of steel structures, such as offshore platforms or ship hulls, necessitating proper corrosion protection measures to mitigate the detrimental impact. The structural steel S275 is used in our study for referring to real-life applications.

4 Conclusions

The long-term consequence of heat treatment on the corrosion behavior of S275 steel was studied using accelerated corrosion with different exposure times. The corrosion rate

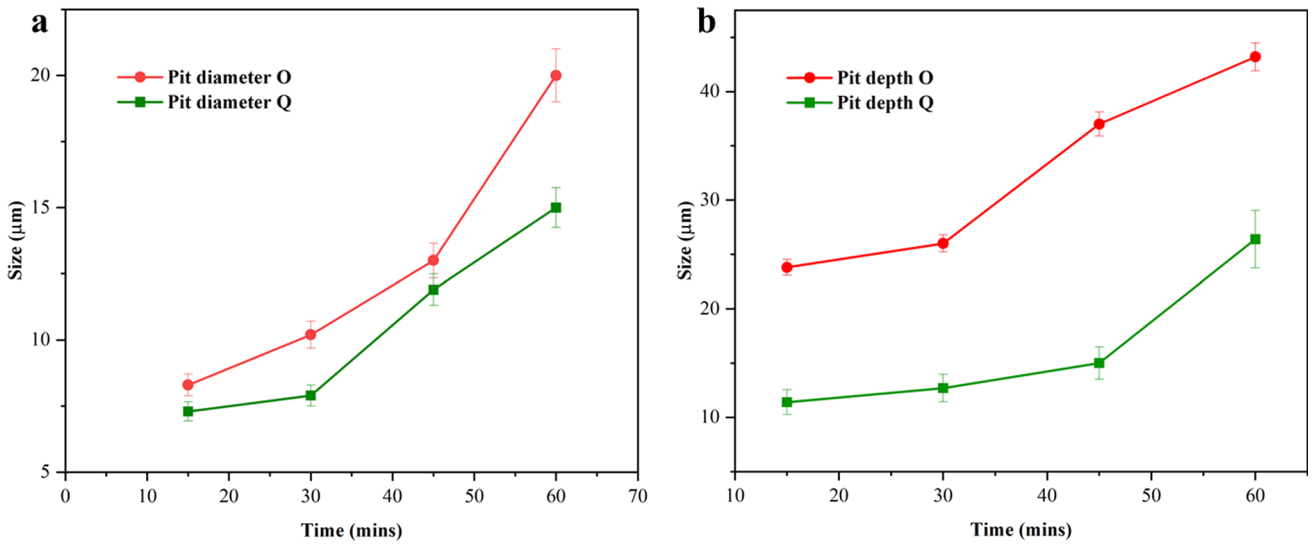

Fig. 8 Variation in **a** pit diameter and **b** pit depth with respect to exposure time

showed negligible difference with no applied voltage and low exposure time for the original and the quenched samples. However, with increased exposure time, the corrosion rate changed drastically. The smaller pits formed on the originalsamples acted as cathodic reaction centers, further aggravating corrosion. The corrosion rate of the original samples ranged from 0.8 to 7.8 mmpy; while, the corrosion rate of the quenched samples did not change much from 0.8 mmpy, showing the effect of quenching to withhold long-term corrosion. The small grain size with the uniform alignment of the quenched samples prevented the ions, generated by the external voltage, from causing reactions leading to corrosion. Future studies should analyze the surface changes over extended periods and different environments to corroborate the observed effectiveness of quenching in reducing corrosion rates. Additionally, continuous examination of the formation and evolution of corrosion products can provide deeper insights into the mechanisms driving the differences between original and quenched samples over a long period of time.

Funding The authors declare that no funds, grants, or other support were received during the preparation of this manuscript.

Data Availability The datasets generated during and/or analyzed during the current study are available from the corresponding author on reasonable request.

Declarations

Competing interests The authors have no relevant financial or non-financial interests to disclose.

References

1. Jaafar, N.; Abdullah, A.; Samad, Z.: Effect of punching die angular clearance on punched hole quality of S275 mild steel sheet metal. Int. J. Adv. Manuf. Technol. **101**, 1553–1563 (2019)
2. Krolo, P.; Grandić, D.; Smolčić, Ž: Experimental and numerical study of mild steel behaviour under cyclic loading with variable strain ranges. Adv. Mater. Sci. Eng. **2016**, 1–13 (2016)
3. Aldeeb, T.; Abduelmula, M.: Fatigue strength of S275 Mild Steel under cyclic loading. Int. J. Mater. Metall. Eng. **12**(10), 564–570 (2018)
4. Mercer, A.; Lumbard, E.: Corrosion of mild steel in water. Br. Corros. J. **30**(1), 43–55 (1995)
5. Melchers, R.E.; Jeffrey, R.: Early corrosion of mild steel in seawater. Corros. Sci. **47**(7), 1678–1693 (2005)
6. Araoyinbo, A.O.; Samuel, A.; Abdullah, A.M.M.; Biodun, M.: The effect of quenching on high-temperature heat treated mild steel and its corrosion resistance. Pertan. J. Sci. Technol. **30**(1), 291–302 (2022)
7. Harsimran, S.; Santosh, K.; Rakesh, K.: Overview of corrosion and its control: a critical review. Proc. Eng. Sci **3**(1), 13–24 (2021)
8. De la Fuente, D.; Díaz, I.; Simancas, J.; Chico, B.; Morcillo, M.: Long-term atmospheric corrosion of mild steel. Corros. Sci. **53**(2), 604–617 (2011)
9. Lalvani, S.; Zhang, G.: The corrosion of carbon steel in a chloride environment due to periodic voltage modulation: Part I. Corros. Sci. **37**(10), 1567–1582 (1995)

10. Tang, K.: Corrosion of steel fibre reinforced concrete (SFRC) subjected to simulated stray direct (DC) interference. Mater.Today Commun. **20**, 100564 (2019)
11. Tang, K.: Stray alternating current (AC) induced corrosion of steel fibre reinforced concrete. Corros. Sci. **152**, 153–171 (2019)
12. Kim, S.-K., et al.: Bimetallic nanocatalysts immobilized in nanoporous hydrogels for long-term robust continuous glucose monitoring of smart contact lens. Adv. Mater. **34**(18), 2110536 (2022). https://doi.org/10.1002/adma.202110536
13. Parapurath, S.; Jacob, L.; Gunister, E.; Vahdati, N.: Effect of microstructure on electrochemical properties of the EN S275 mild steel under chlorine-rich and chlorine-free media at different pHs. Metals **12**(8), 1386 (2022)
14. Boschmann Käthler, C.; Poulsen, S.L.; Sørensen, H.E.; Angst, U.M.: Investigations of accelerated methods for determination of chloride threshold values for reinforcement corrosion in concrete. Sustain. Resil. Infrastruct. **8**(2), 197–208 (2023). https://doi.org/10.1080/23789689.2021.1905221
15. Feng, W.; Dong, Z.; Liu, W.; Cui, H.; Tang, W.; Xing, F.: An experimental study on the influence of applied voltage on current efficiency of rebars with a modified accelerated corrosion test. Cem. Concr Compos. **122**, 104120 (2021). https://doi.org/10.1016/j.cemconcomp.2021.104120
16. Katiyar, P.K.; Misra, S.; Mondal, K.: Comparative corrosion behavior of five microstructures (Pearlite, Bainite, Spheroidized, Martensite, and tempered Martensite) made from a high carbon steel. Metall. Mater. Trans. A **50**(3), 1489–1501 (2019). https://doi.org/10.1007/s11661-018-5086-1
17. Osório, W.; Peixoto, L.; Garcia, L.; Garcia, A.: Electrochemical corrosion response of a low carbon heat treated steel in a NaCl solution. Mater. Corros. **60**(10), 804–812 (2009)
18. Soleimani, M.; Mirzadeh, H.; Dehghanian, C.: Effect of grain size on the corrosion resistance of low carbon steel. Mater. Res. Exp. **7**(1), 016522 (2020). https://doi.org/10.1088/2053-1591/ab62fa
19. Krishnan, S.; Dumbre, J.; Bhatt, S.; Akinlabi, E.T.; Ramalingam, R.: Effect of crystallographic orientation on the pitting corrosion resistance of laser surface melted AISI 304L austenitic stainless steel. Int. J. Mech. Aerosp. Indus. Mech. Eng. **7**(4), 239–242 (2013)
20. DelVecchio, E.; Liu, T.; Chang, Y.-T.; Nie, Y.; Eslami, M.; Charpagne, M.A.: Metastable cellular structures govern localized corrosion damage development in additive manufactured stainless steel. npj Mater. Degrad. **8**(1), 45 (2024). https://doi.org/10.1038/s41529-024-00464-8
21. Cruz, R.P.V.; Nishikata, A.; Tsuru, T.: AC impedance monitoring of pitting corrosion of stainless steel under a wet-dry cyclic condition in chloride-containing environment. Corros. Sci. **38**(8), 1397–1406 (1996). https://doi.org/10.1016/0010-938X(96)00028-5
22. Hœrlé, S.; Mazaudier, F.; Dillmann, P.; Santarini, G.: Advances in understanding atmospheric corrosion of iron. II. Mechanistic modelling of wet–dry cycles. Corros. Sci. **46**(6), 1431–1465 (2004)
23. Stratmann, M.; Müller, J.: The mechanism of the oxygen reduction on rust-covered metal substrates. Corros. Sci. **36**(2), 327–359 (1994)
24. Dong, C.F.; Fu, A.Q.; Li, X.G.; Cheng, Y.F.: Localized EIS characterization of corrosion of steel at coating defect under cathodic protection. Electrochim. Acta **54**(2), 628–633 (2008). https://doi.org/10.1016/j.electacta.2008.07.016
25. Melchers, R.E.: 9 - Modelling long term corrosion of steel infrastructure in natural marine environments. In: Liengen, T.; Féron, D.; Basséguy, R.; Beech, I.B. (Eds.) Understanding Biocorrosion, pp. 213–241. Woodhead Publishing, Oxford (2014)
26. Alcántara, J.; de la Fuente, D.; Chico, B.; Simancas, J.; Díaz, I.; Morcillo, M.: Marine atmospheric corrosion of carbon steel: a review. Materials **10**(4), 406 (2017)
27. Melchers, R.E.: Nonlinear trending of corrosion of high nickel alloys in extended marine and atmospheric exposures. Corros. Rev. **38**(6), 515–528 (2020). https://doi.org/10.1515/corrrev-2020-0079
28. Melchers, R.E.: A review of trends for corrosion loss and pit depth in longer-term exposures. Corros. Mater. Degrad. **1**(1), 42–58 (2020)
29. Jeffrey, R.; Melchers, R.E.: The changing topography of corroding mild steel surfaces in seawater. Corros. Sci. **49**(5), 2270–2288 (2007). https://doi.org/10.1016/j.corsci.2006.11.003
30. Steigerwald, R.; Greene, N.: The anodic dissolution of binary alloys. J. Electrochem. Soc. **109**(11), 1026 (1962)
31. Demircioğlu, A.; Demir, K.Ç.: Effects of annealing on structural, morphological, and corrosion properties of α-Fe_2O_3 thin films. J Electron Mater **50**(5), 2750–2760 (2021). https://doi.org/10.1007/s11664-021-08786-y
32. Jiang, B.; Doi, K.; Tsuchiya, K.; Kawano, Y.; Kori, A.; Ikushima, K.: Micromechanical properties of steel corrosion products in concrete studied by nano-indentation technique. Corros Sci **163**, 108304 (2020). https://doi.org/10.1016/j.corsci.2019.108304
33. de la Fuente, D.; Alcántara, J.; Chico, B.; Díaz, I.; Jiménez, J.A.; Morcillo, M.: Characterisation of rust surfaces formed on mild steel exposed to marine atmospheres using XRD and SEM/Micro-Raman techniques. Corros. Sci. **110**, 253–264 (2016). https://doi.org/10.1016/j.corsci.2016.04.034
34. Bajt Leban, M.; Kosec, T.: Characterization of corrosion products formed on mild steel in deoxygenated water by Raman spectroscopy and energy dispersive X-ray spectrometry. Eng. Fail. Anal. **79**, 940–950 (2017). https://doi.org/10.1016/j.engfailanal.2017.03.022
35. Chicot, D., et al.: Mechanical properties of magnetite (Fe_3O_4), hematite (α-Fe_2O_3) and goethite (α-FeO·OH) by instrumented indentation and molecular dynamics analysis. Mater. Chem. Phys. **129**(3), 862–870 (2011). https://doi.org/10.1016/j.matchemphys.2011.05.056
36. de Faria, D.L.A.; Venâncio Silva, S.; de Oliveira, M.T.: Raman microspectroscopy of some iron oxides and oxyhydroxides. J. Raman Spectrosc. **28**(11), 873–878 (1997)
37. Stringer, R.; Johnston, P.: Chlorine and the environment: an overview of the chlorine industry. Springer Netherlands, Dordrecht (2001)
38. Tait, W.S.: Electrochemical corrosion basics. In: Handbook of environmental degradation of materials, pp. 97–115. Elsevier, Hoboken (2018)
39. Ahmad, S.: Techniques for inducing accelerated corrosion of steel in concrete. Arab. J. Sci. Eng. **34**(2), 95 (2009)
40. Gan, F.; Sun, Z.-W.; Sabde, G.; Chin, D.-T.: Cathodic protection to mitigate external corrosion of underground steel pipe beneath disbonded coating. Corrosion **50**(10), 804–816 (1994)